

Pairwise-Rotated EOFs of Global SST

XIANYAO CHEN

Physical Oceanography Laboratory/CIMST, Ocean University of China, and Qingdao National Laboratory of Marine Science and Technology, Qingdao, China

JOHN M. WALLACE

Department of Atmospheric Sciences, University of Washington, Seattle, Washington

KA-KIT TUNG

Department of Applied Mathematics, University of Washington, Seattle, Washington

(Manuscript received 1 November 2016, in final form 4 April 2017)

ABSTRACT


Empirical orthogonal function (EOF) analysis of global sea surface temperature yields modes in which interannual variability associated with ENSO and the lower-frequency variability associated with the Pacific decadal oscillation (PDO) and the Atlantic multidecadal oscillation (AMO) are confounded with one another and with the signature of global warming. The confounded EOFs exhibit overlapping centers of action with polarities of the perturbations juxtaposed such that the respective modes are mutually orthogonal in the global domain. When physical modes with different time scales appear in the same pair of EOFs, the principal component (PC) time series tend to be positively correlated in one frequency band and negatively correlated in another. Mode mixing may be a reflection of sampling variability or it may reflect the lack of spatial orthogonality of the physical modes themselves. Using sequences of pairwise orthogonal rotations of selected PCs, it is possible, without recourse to filtering, to recover a global warming mode with a bland spatial pattern and a nearly linear upward trend, along with dynamical modes, each with its own characteristic time scale, that resemble ENSO, the PDO, and the AMO. Novel elements of this analysis include a rationale for choosing the optimal angle for pairwise rotation and a simple algorithm for eliminating mode mixing between the dynamical modes and the global warming mode by transferring the linear trends from the former to the latter.

1. Introduction

A plethora of modes of variability of sea surface temperature (SST) have been identified through a variety of analysis protocols, some relating to the global SST and others to SST in regional domains; some based on raw data and others on data filtered a priori to emphasize particular frequency ranges; some based on SST itself and others on pointwise detrended SST or residual SST after subtracting out the time-varying global mean SST at each grid point (hereafter referred to as SST*); and some using conventional EOFs and others using

rotated EOFs and other variants of EOF analysis, as summarized in Table 1. Modes that have emerged in these analyses include the signature of human-induced global warming (Latif et al. 1997; Folland et al. 1999; Yeo et al. 2017), El Niño–Southern Oscillation (ENSO; Weare et al. 1976; Zhang et al. 1997), the Pacific decadal oscillation (PDO; Mantua et al. 1997; Minobe 1999), the interdecadal Pacific oscillation (IPO; Folland et al. 1999), and the Atlantic multidecadal oscillation (AMO; Enfield et al. 2001; Guan and Nigam 2009; Schlesinger and Ramankutty 1994; Trenberth and Shea 2006).

In conventional (i.e., unrotated) EOF expansions two or more physical modes of variability often appear in linear combination in the same mathematical (EOF) mode, with their polarities juxtaposed in such a way that the modes are spatially orthogonal in the domain of the analysis. Orthogonal modes may occur in linear combination in a pair of EOFs when the eigenvalues of the

 Denotes content that is immediately available upon publication as open access.

Corresponding author: Xianyao Chen, chenxy@ouc.edu.cn

TABLE 1. EOF analysis of global and regional SST. A dash indicates no further preprocessing, including filtering or linear detrending, was performed. (HSSTD: historical SST database, CEOF: complex EOF analysis, PLD: pointwise linearly detrended, MSSA: multi-channel singular spectrum analysis, REOF: rotated EOF, CSEOF: cyclostationary EOF analysis, POP: principal oscillation pattern, MCA: maximum covariance analysis, REEOF: rotated extended EOF analysis, SSA: singular spectrum analysis, and EEOF: extended EOF analysis; additional acronym expansions available online at <http://www.ametsoc.org/PubsAcronymList>.)

Reference	Dataset	Period of record	Domain	Time resolution	Type of analysis	Filtering	Trend treatment
Folland et al. (1999)	Met Office Hadley Centre SST	1911–95	Global	Seasonal	EOF	13.3-yr low pass	—
Enfield and Mestas-Núñez (1999)	Kaplan SST	1856–1991	Global	Monthly	CEOEF	8-yr low pass	PLD
Barcikowska et al. (2017)	HadISST–ERSST.v4	1876–2015	Global	Monthly	MSSA	70-yr lagged window	—
Mestas-Núñez and Enfield (1999)	Kaplan SST	1856–1991	Global	Monthly	REOF	8-yr low pass	PLD
McCabe and Palecki (2006)	Kaplan	1925–2003	Global	Monthly	EOF	10-yr low pass	PLD
Parker et al. (2007)	HadCRUT3	1891–2005	Global	Seasonal	EOF	11-yr low pass	—
Tourre et al. (2010)	GISST	1900–2000	Global	Monthly	EOF	30-yr low pass	—
Yeo et al. (2017)	ERSST.v3b	1872–2015	Global	Monthly	CSEOF	—	—
Chiang and Vimont (2004)	NCEP–NCAR	1948–2001	Tropical Pacific, tropical Atlantic	Monthly	MCA	3-month running mean	PLD
Guan and Nigam (2009)	HadISST	1901–2006	Pacific, Atlantic	Seasonal	REOF	Filtered Pacific modes	PLD
Deser et al. (2010)	HadISST	1900–2008	Multiple regions	Monthly	EOF	—	PLD
Messié and Chavez (2011)	ERSST.v3b	1910–2009	Multiple regions	Monthly	EOF	—	PLD
Mantua et al. (1997)	HSSTD	1900–93	North Pacific	Monthly	EOF	—	SST*
Zhang et al. (1997)	HSSTD	1900–93	Pacific	Monthly	EOF	6-yr high pass	SST*
Latif et al. (1997)	GISST	1949–91	Pacific	Monthly	POP-EOF	5-month running mean	PLD
Barlow et al. (2001)	COADS	1945–93	Pacific	Monthly	REOF	—	—
Newman et al. (2003)	HadISST	1900–99	Pacific	Monthly	EOF	—	—
Guan and Nigam (2008)	HadISST	1900–2002	Pacific	Seasonal	REEOF	—	—
Zhang et al. (2010)	HadISST	1870–2006	Tropical Pacific	Monthly	EOF	—	—
Takahashi et al. (2011)	HadISST	1870–2010	Tropical Pacific	Monthly	REOF	—	—
Lian and Chen (2012)	HadISST	1948–2007	Tropical Pacific	Monthly	REOF	—	—
Chen and Wallace (2015)	ERSST.v3b	1900–2013	Pacific	Monthly	EOF	—	SST*
Deser and Blackmon (1993)	COADS	1900–89	Atlantic	Seasonal	EOF	—	—
Shapiro and Goldenberg (1998)	COADS	1968–92	Atlantic	Monthly	EOF	—	PLD
Czaja and Frankignoul (2002)	NCEP–NCAR	1958–97	Atlantic	Monthly	MCA	Third-order polynomial low pass	PLD
Jamison and Kravtsov (2010)	Kaplan–HadISST	1856–2007	Atlantic	Monthly	EOF-SSA	—	PLD
Nigam et al. (2011)	HadISST	1900–2009	Atlantic	Monthly	EEOF	Filtered ENSO-like modes	PLD

mathematical modes are not sufficiently well separated (North et al. 1982; Quadrelli et al. 2005). But a more fundamental cause of mode mixing is the fact that the physical modes of variability are not constrained to be spatially orthogonal within a prescribed analysis domain. This “structural mode mixing” can occur even when the eigenvalues are well separated and the EOFs are robust

(i.e., not subject to large sampling variability arising from factors such as which dataset, what period of record, or what sampling interval is used in the analysis).

Telltale indicators of mode mixing of either kind are spatially dependent or frequency-dependent temporal correlations. An example of the former is collocated centers of action, one or more of which appear with the

same sign and one or more with opposing sign, such that the two EOFs exhibit a mathematically contrived spatial orthogonality within the domain of the analysis. But mode mixing is not always so obvious in the spatial patterns, especially in EOFs with nonzero spatial means. Frequency-dependent temporal correlations may manifest themselves as

- 1) trends of like sign with correlations of opposing sign in the variability about their trend lines (or trends of opposing sign with correlations of like sign in the variability about their trend lines) or
- 2) correlations of opposing sign in different frequency ranges.

An example of the first is the mixing between ENSO and global warming signatures in the two leading EOFs of SST in the tropical Pacific domain (Zhang et al. 2010), and an example of the second is the mixing between ENSO and the PDO in the two leading modes of SST* in the pan-Pacific domain (Chen and Wallace 2016, hereafter CW16).

The need for rotating the EOFs to eliminate mode mixing has been discussed and debated in many previous studies. Notable examples are the exchange between Richman (1986) and Jolliffe (1987) and, with specific reference to global SST patterns, the more recent study of Lian and Chen (2012, hereafter LC12). By far the most widely used rotation algorithm in climate studies is to use varimax rotation of a subset of the modes to simplify their spatial patterns; that is, to maximize the kurtosis of the EOFs such that their dominant “centers of action” tend to be emphasized at the expense of the weaker ones, while retaining the orthogonality of the principal components (PCs) (Kaiser 1958; Richman 1986; Wilks 2011). This protocol requires one choice on the part of the analyst—the number of modes to rotate—and the results are not unduly sensitive to this choice provided that the number of modes included in the rotation is large enough. Varimax rotation yields robust modes that are often easier to interpret than the conventional EOFs. A notable example is the way it reduces mode mixing between global warming and ENSO (LC12).

An alternative approach to improving the correspondence between the EOFs and the physical modes of variability is to pairwise rotate the mixed modes. Orthogonal rotation of a pair of (standardized) PCs, PC_i and PC_j , through angle θ , yields

$$RPC_i = \cos\theta PC_i - \sin\theta PC_j$$

and

$$RPC_j = \sin\theta PC_i + \cos\theta PC_j.$$

When the EOFs are rotated through the same angle, the PCs retain their temporal orthogonality after rotation in accordance with the above formula, while the corresponding spatial patterns (EOFs), like the physical modes that they are intended to represent, are not constrained to remain mutually orthogonal.

Selective pairwise rotation is used routinely in studies of the Madden–Julian oscillation (MJO) and other quasi-periodic phenomena to document how the patterns evolve over the course of one cycle (e.g., Wheeler and Hendon 2004). It is only recently that it has been used for the purpose of eliminating mode mixing. In their investigation of patterns of SST* variability in the tropical Pacific domain, Takahashi et al. (2011) and Dommenges et al. (2013) rotated the two leading EOFs of tropical Pacific SST*. CW16 rotated the two leading EOFs of pan-Pacific SST* to transform their principal components into orthogonal indices, one representing an equatorial ENSO mode in which the variance is more concentrated on the interannual time scale, and the other a PDO-like pan-Pacific mode with more variability on the decadal time scale. All three of these studies employed 45° rotations.

Here we present an analysis of the EOFs and PCs of the nondetrended, global SST field, using selected pairwise rotations to eliminate mode mixing, and choosing the rotation angle objectively, on the basis of metrics that are to be minimized. The study is based mainly on SST from Extended Reconstructed Sea Surface Temperature, version 3b (ERSST.v3b; Smith et al. 2008), analysis from the NOAA/Climate Prediction Center for the period of record 1910–2015. All data are SST anomalies (departures from climatological means for each calendar month).

In the next section we will describe and justify the pairwise rotation protocol used in this study, including the choice of rotation angle, thereby providing a “road map” for the results section that follows. We will show results based on two variants of the dataset: unfiltered monthly mean data and 3-month running mean data, which we will refer to as seasonal mean data. The final rotated results are robust despite differences in the intermediate steps. The results section also includes a brief exploration of Atlantic–Pacific coupling based on the EOFs of filtered data and an analysis of the contributions of the rotated EOFs to variations in global mean SST. In the final section we summarize and interpret the results and document their robustness with respect to sampling variability.

2. Pairwise rotation

In contrast to varimax rotation, which can be viewed as a single operation that requires no further intervention on the part of the analyst once he/she has

decided how many modes to rotate, the analysis protocol that we envision involves a series of pairwise rotations that need to be monitored by the analyst or performed in accordance with a set of rules specified in advance. The pairwise rotations are performed to eliminate mode mixing between (i) the global warming trend and dynamical modes of variability such as ENSO and (ii) different dynamical modes of variability. Dealing with mode mixing resulting from sampling variability first puts the remainder of the analysis on a firmer footing. We have determined that the final results are not sensitive to the order in which (i) and (ii) are performed. Now let us consider the choice of optimal rotation angle for extricating physical modes from EOFs in which they appear in linear combination with one another.

a. Criteria for choosing the optimal rotation angle

In previous studies in which pairwise rotation has been used to eliminate mode mixing, the EOFs were rotated through a 45° angle, which is equivalent to replacing the standardized PCs by their sums and differences, divided by the normalization factor $\sqrt{2}$. By construction, the rotated modes account for equal fractions of the total variance. No justification for this choice has been offered in these antecedent studies, apart from mathematical symmetry and the desirable characteristics of the rotated modes.

For pairwise rotations between different dynamical modes of variability, there are a number of different criteria that could be used for choosing the optimal rotation angle. Here we will consider just two of them: one relating to the spatial patterns of the EOFs and the other to the time-dependent behavior of the PCs. For rotations based on both of these criteria, the orthogonality of the EOFs is relaxed while the PCs retain their orthogonality, and the PCs are standardized to unit variance while the EOFs are not standardized. These practices are consistent with most previous studies.

The spatial criterion minimizes the squared (temporal) covariance between the gridpoint values of EOFs, area averaged over the domain of the analysis [i.e., the spatially averaged squared covariance (SASC)]—a measure of the prominence of collocated centers of action in the pair of EOFs. It can be shown that the minimum SASC occurs at the same angle as the maximum in the sum of the kurtosis of the two EOFs. Hence, rotation in accordance with the SASC criterion can be viewed as a form of pairwise varimax rotation with appropriate scaling.

The other criterion involves minimizing the frequency-dependent (temporal) covariances between the detrended PCs in the interannual (less than 6-yr period), decadal (6–20-yr period), and multidecadal (greater than

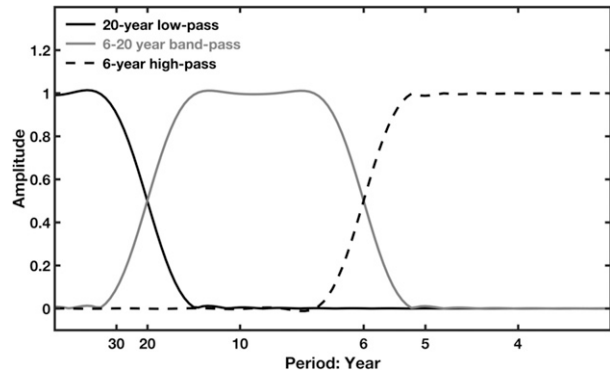


FIG. 1. Frequency response functions of 6-yr high-pass, 6–20-yr bandpass, and 20-yr low-pass Lanczos filters used to separate the interannual, decadal, and multidecadal variability in certain time series in this paper.

20-yr period) frequency bands, as defined by the Lanczos filters whose frequency responses are shown in Fig. 1. We compute the squared covariances for each of the three bands and sum them to obtain the frequency-averaged squared covariance (FASC).

In choosing the optimal rotation angle for rotations performed for the purpose of separating the global warming mode (GW) from the dynamical modes of variability such as ENSO, we assume that the dynamical modes do not exhibit significant linear trends of their own. Accordingly, for each of the predominantly “dynamical” PCs (2–4), we define the optimal angle as the one that will transfer its linear trend to the global warming mode PC1, thereby detrending it. This is accomplished by rotating each of them with PC1 through the angle θ , whose tangent is the ratio of the trend in their PC to the trend in PC1. The pairwise rotations are performed sequentially; that is, the previously rotated PC1 is rotated with the next dynamical PC to ensure that orthogonality is maintained. The order in which the dynamical PCs are rotated with PC1 does not affect the final result.

b. The analysis protocol

Figure 2 shows a “road map” through the rotations performed on the unfiltered monthly mean global SST anomaly data, starting with the conventional (unrotated) EOF1–4 in (i) of Fig. 2. We will show that the spatial patterns of EOF3 and EOF4 in the unfiltered monthly mean data exhibit collocated centers of action, a telltale sign of mode mixing. That the eigenvalues of these two modes account for nearly identical fractions of the variance indicates that this mode mixing is likely a manifestation of sampling variability of the kind described by North et al. (1982). These modes are pairwise rotated to obtain a more robust set of EOFs, as depicted in (ii) of Fig. 2. EOF1 is identified as the mode

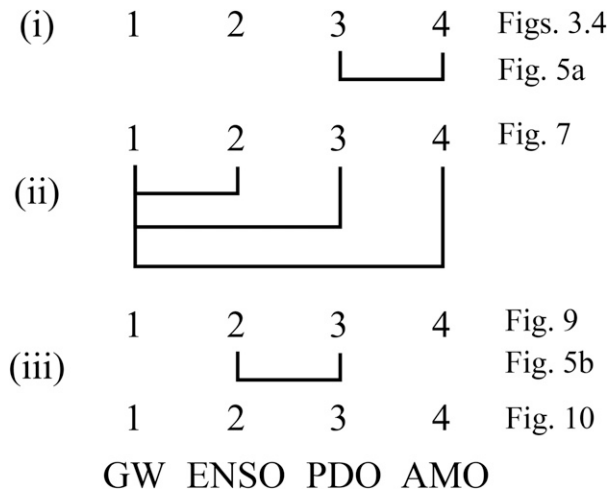


FIG. 2. Overview of the rotations performed in sections 3a–c. The labels (i), (ii), and (iii) indicate the order in which the rotations are performed in this paper.

that carries most of the global warming signal but the predominantly dynamical modes 2–4 also exhibit trends. The “trend transfer algorithm” described in the previous section is applied to detrend PC2–4. The resulting

PCs are depicted in (iii) of Fig. 2. There remains evidence of mode mixing between the two Pacific modes, which is eliminated by means of another pairwise rotation, with the angle chosen in accordance with the FASC metric criterion. This final step yields the modes depicted in (iii) of Fig. 2, which resemble modes identified in previous studies, as indicated. If the SASC metric is used in choosing the angle in the final rotation, a somewhat different solution is obtained.

When EOF analysis is performed on the seasonal mean (i.e., 3-month running mean filtered) data, there is no evidence of mode mixing in the relationships between their spatial patterns in the Atlantic and the Pacific in (i) of Fig. 2, perhaps because the eigenvalues of their third and fourth modes are more widely separated. Accordingly, we proceed directly to rotations to eliminate the trends in modes 2–4. The final results are virtually identical to those based on the unfiltered monthly data.

3. Results

The four leading (unrotated) EOFs and PCs of global SST based on seasonal and monthly mean data are

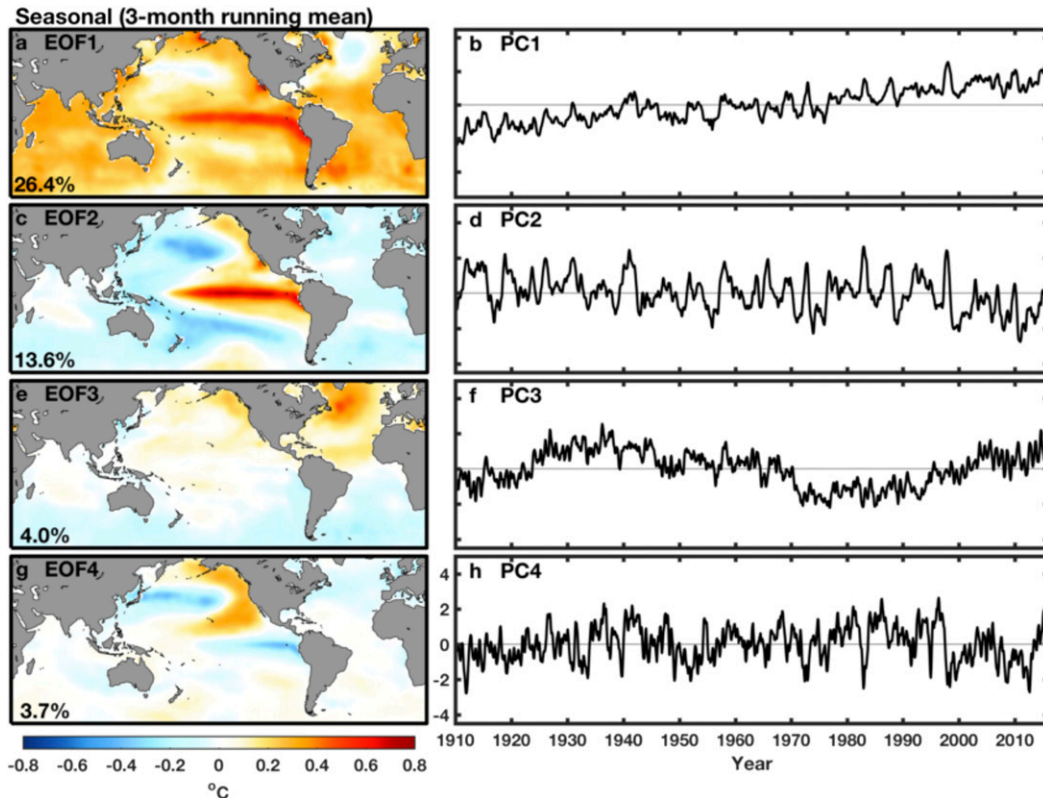


FIG. 3. Conventional (i.e., unrotated) EOFs and PCs of seasonal mean (i.e., 3-month running mean) global SST based on ERSST.v3b for the period of record 1910–2015. Percentages of explained variance are printed at the bottom left on the EOF maps.

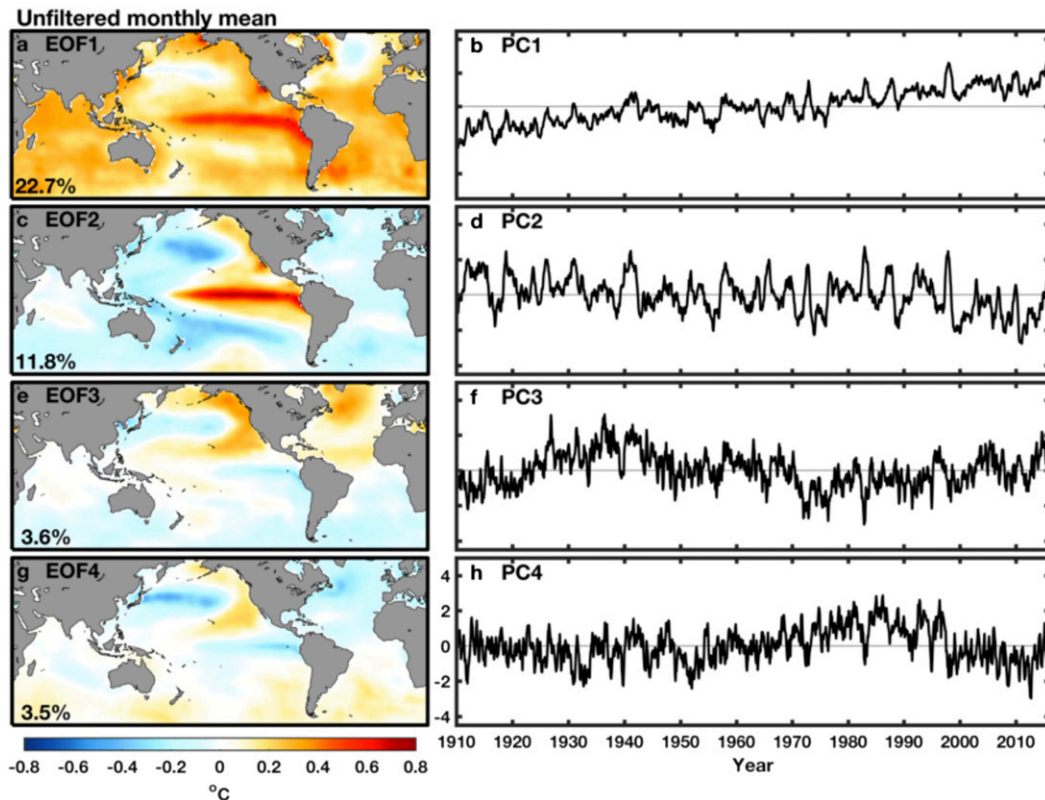


FIG. 4. As in Fig. 3, but for monthly mean global SST.

shown in Figs. 3 and 4, respectively. The two leading modes are virtually identical, apart from the fact that they explain slightly larger fractions of the variance of the seasonal mean data. In contrast, the third and fourth modes are quite different. In the EOFs derived from the seasonal mean data they take the form of nearly separate Pacific and Atlantic patterns, whereas in the EOFs derived from the monthly mean data the Atlantic and Pacific patterns are mixed. We hypothesize that this difference is due to the fact that the eigenvalues of the third and fourth eigenvalues (as inferred from the percentage of explained variances shown in Figs. 3 and 4) are not well separated, especially for the monthly mean data. In any case, it is clear from visual inspection and from an evaluation of the SASC and FASC metrics that EOF3 and EOF4 of the monthly data mean are mixed, while those of the seasonal mean data are not.

a. Rotating EOF3 and EOF4 of the monthly mean data

To determine the optimal angle for rotating EOF3 and EOF4 of the monthly mean data, we tried using both SASC and FASC metrics. Values of the two metrics for monthly PC3 and PC4 are plotted in Fig. 5a as a function of rotation angle. They both vary nearly sinusoidally,

with minima close to 42° . The pairwise-rotated modes for that rotation angle, shown in Fig. 6, are seen to be very similar to their counterparts derived directly from the seasonal mean data. From here onward we will consider only the EOFs of the seasonal mean data shown in Fig. 3 unless otherwise noted.

b. Trend transfer

Next we transfer the linear trends in PC2–4 to PC1 using the algorithm described in the previous section. The rotation angles are 23° , 12° , and -3° , respectively, and the transformed modes after the three pairwise rotations are shown in Fig. 7. Pairwise rotation with EOFs and PC2–4 removes the prominent ENSO signature in EOF1, leaving a pattern that is even more spatially uniform than the pattern derived by regressing global SST upon its own spatial average (GSST; not shown). The rotated PC1 is dominated by the linear upward global warming trend to a greater degree than it was before the rotations. EOF2–4 are much less strongly affected by the rotation and, apart from the detrending, their PCs are virtually unchanged.

Figure 8 provides further specifics on how these pairwise-rotated PCs relate to the time series of GSST, with emphasis on the departures from a linear upward

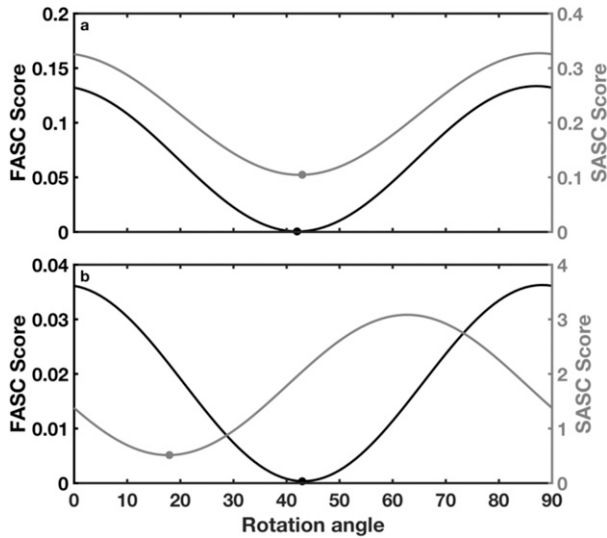


FIG. 5. The SASC metric (gray curves) and FASC metric (black curves) plotted as a function of rotation angle. (a) The pairwise rotation between PC3 and PC4 of the monthly mean data [step (i) as described in the overview in Fig. 2] before the trends have been transferred to PC1, and (b) the pairwise rotation between PC2 and PC4 (i.e., the Pacific modes) of the seasonal mean data after the trends have been transferred to PC1 [step (ii) as described in the overview in Fig. 2].

trend. The top pair of time series is detrended GSST and sum of the rotated PC1–4 scaled by the global means of the respective EOFs. That the two curves are virtually identical proves that the four leading modes considered in this study are sufficient to explain the contribution of dynamical modes of variability in SST to variations in the rate of rise of GSST.

The remaining curves in Fig. 8 show the individual contributions of rotated EOF1–4 to detrended GSST. They are same as the standardized PCs, scaled by the global means of the respective EOFs. The EOF1

contribution is dominated by the abrupt drop in 1945, an artifact of the transition of SST measurements from bucket temperatures to condenser intake temperatures (Thompson et al. 2008). Smaller dips following the eruptions of Mt. Agung (1963/64) and Mt. Pinatubo (1991) are also discernible. That the variance of the first mode is substantially smaller than that of GSST itself reflects the dynamical contribution to temporal variations in GSST embodied the curves for EOF2–4. The GSST time series can be transformed so that it closely matches the rotated EOF1 contribution by 1) linearly detrending it, 2) regressing out PC2–4, 3) summing the linear trend and the residual time series, and 4) standardizing.

The EOF4 contribution to the variability of GSST in Fig. 8 is seen to be negligible. Hence, to a close approximation, the dynamical contribution to variations in GSST from SST variability in the Pacific sector is represented by the EOF2 contribution and that from the Atlantic sector by the EOF3 contribution. The time scales of the Pacific and Atlantic contributions are dramatically different. We will offer further insights into the dynamical contribution in section 3e after performing a further pairwise rotation of EOF2 and EOF4.

c. Rotation of the Pacific modes

After pairwise rotation with EOF1, we find that EOF2 and EOF4 of global SST closely resemble unrotated EOF1 and EOF2 of pan-Pacific SST* shown in Fig. 1 of CW16. The collocated eastern equatorial Pacific and central North Pacific centers of action in the two patterns are indicative of mode mixing. Another indicator is the fact that the correlation between their PCs is frequency dependent: 0.62 for the decadal band and –0.17 for the interannual band, both of which are statistically significant at the 95% confidence level, based on a one-sided

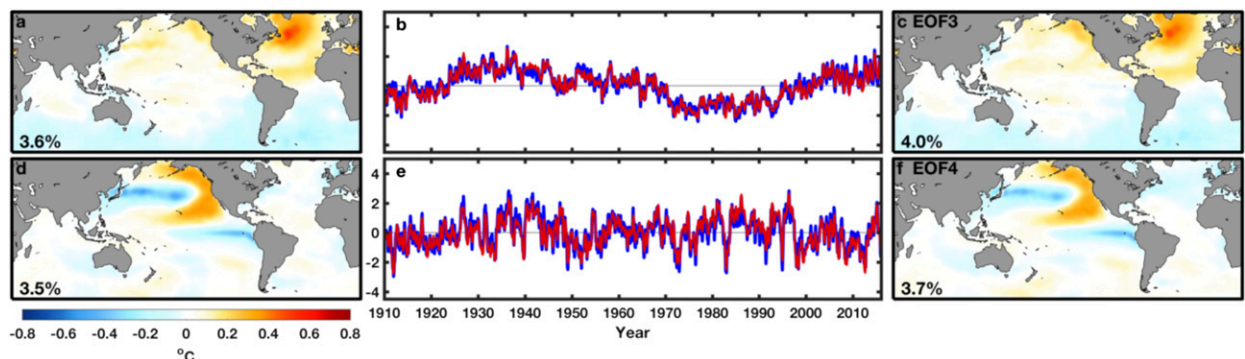


FIG. 6. The 43° pairwise-rotated (a) EOF3 and (d) EOF4 of monthly mean SST. Unrotated (c) EOF3 and (f) EOF4 of seasonal mean (i.e., 3-month running mean) SST repeated from Fig. 3. (b),(e) The corresponding PCs are compared, with the blue line for monthly and the red line for seasonal mean SST. Percentages of explained variance are printed at the bottom left on the EOF maps.

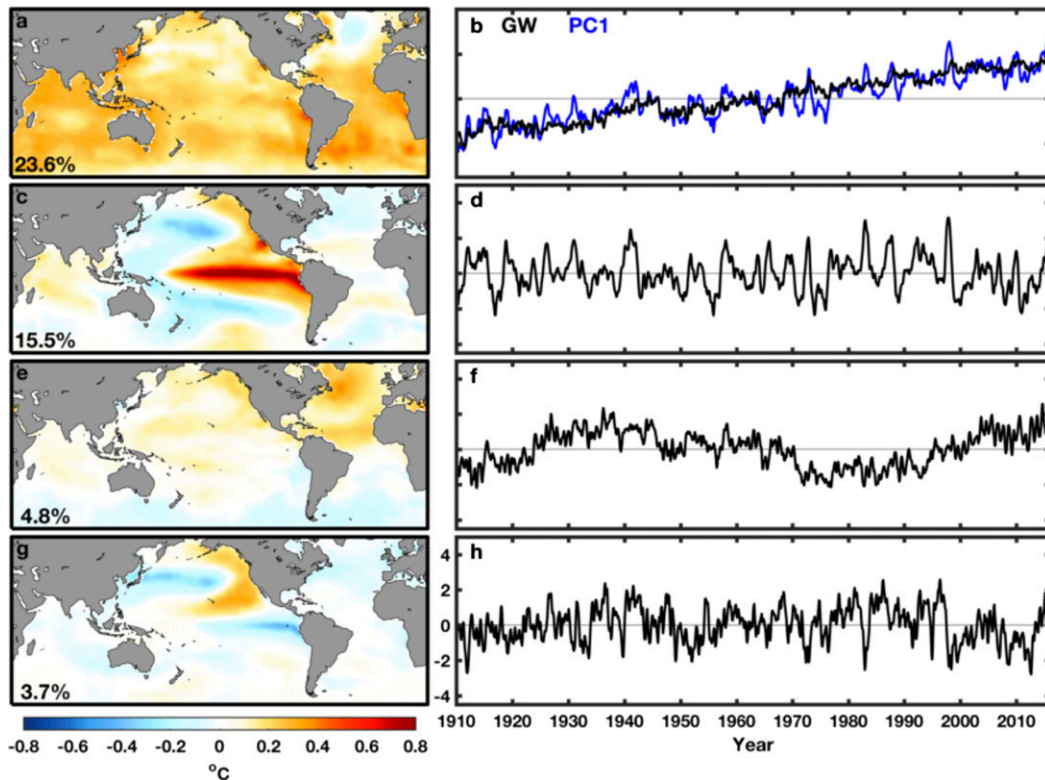


FIG. 7. Pairwise-rotated EOF2, EOF3, and EOF4 after step (ii) in the pairwise rotation protocol outlined in Fig. 2, in which the trends in PC2, PC3, and PC4 are transferred to PC1 but before step (iii) in which EOF2 and EOF3 are rotated, based on seasonal mean (i.e., 3-month running mean) SST. Percentages of explained variance are printed at the bottom left on the EOF maps.

Student's t test, taking into account the autocorrelation (less than a year for the high-frequency band and 8.6 yr for the decadal frequency band), using Eq. (31) of Bretherton et al. (1999). CW16 simplified these patterns by rotating them through an angle of 45° . The optimal rotation angle, as determined by minimizing SASC, is 18° , whereas the value obtained by minimizing FASC is 43° , as shown in Fig. 5b. The pairwise-rotated EOFs for the two angles, shown in Fig. 9, are discernibly different. The modes based on the 43° rotation resemble the PDO-like mode P and the equatorially focused ENSO-like mode T' in CW16. In contrast, the PDO-like mode derived from the 18° rotation lacks the prominent equatorial Pacific signature. It resembles the SST response to the atmospheric PNA pattern, which is evident in lag correlation statistics on time scales as short as a single winter season (Wallace et al. 1990, their Fig. 1). A similar pattern is evident on the interannual time scale in some coupled atmosphere–ocean models in which the ocean is treated as a slab (Dommenget and Latif 2008, their Figs. 2a,b). In some of the CMIP5 simulations summarized in Figs. 8a,b of Newman et al. (2016), the PDO-like mode resembles its counterpart in the 18° rotation, in some it resembles its

counterpart in the 43° rotation, and in most it lies somewhere in between the two.

On the whole, we favor the more expansive mode in the 43° solution based on the FASC criterion because its PC closely resembles the PDO index of Mantua et al. (1997), defined as the leading PC of monthly mean Pacific SST* poleward of 20°N ($r = 0.97$ in 5-month running mean data) and because in nature there is no lack of physically plausible mechanisms capable of producing coupling between tropics and extratropics, as summarized in the recent review article of Newman et al. (2016).

Figures 10a,d,g,j show the pairwise-rotated EOFs after the rotation of the Pacific modes, which marks the final step in the rotation protocol outlined in Fig. 2. They closely resemble the global warming mode and the ENSO-, PDO- and AMO-like modes, respectively. To avoid confusion between mode numbers at various stages of the protocol, we will refer to them by these labels throughout the remainder of this section. The different frequency dependences of the three dynamical modes are clearly revealed by the power spectra of their PCs, displayed on a log period scale in Fig. 11.

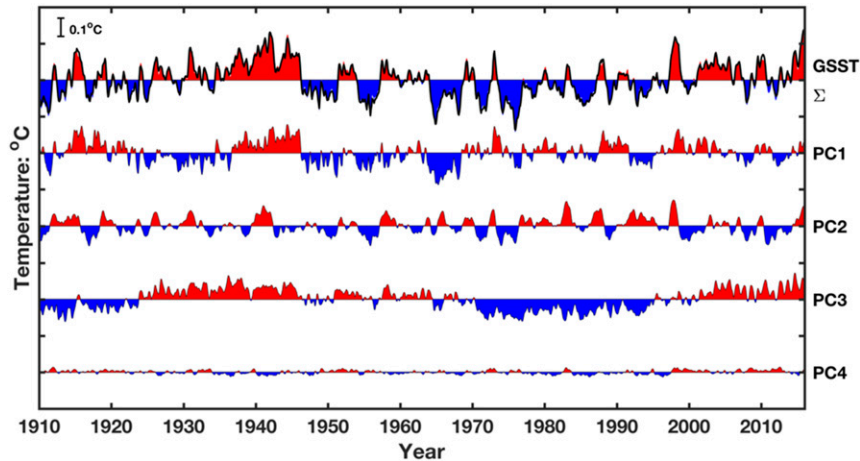


FIG. 8. Time series at top shows linearly detrended global mean SST (GSST; the black line) compared with the sum of rotated PC1–4 labeled by Σ , indicated by the envelope of the colored shading. The other time series are the individual rotated PC1–4 after step (ii) in the rotation protocol outlined in Fig. 2, each scaled in accordance with the global mean of its EOF. Rotated PC1 is detrended for display purposes, to emphasize the variability about its trend line. The temperature scale shown at top left is the same for all curves.

d. Atlantic–Pacific coupling

When plotted on a more sensitive color scale, the AMO-like mode, shown in Fig. 12a, exhibits a weak ENSO- or PDO-like signature: the equatorial Pacific is cold when the Atlantic is warm and vice versa. The negative SST anomalies in the equatorial Pacific cannot be eliminated by pairwise rotation through any prescribed angle (not shown). However, there is no reciprocal AMO-like signature in the PDO-like mode shown in Fig. 13a.

To determine whether the weak Pacific signature in AMO-like mode is a reflection of stronger Atlantic–Pacific coupling on the inter- or multidecadal time scale that is diluted by the presence of more local (intraocean) higher-frequency variability, we performed EOF

analysis followed by the same pairwise rotation protocol on 3-, 6-, 12-, and 20-yr low-pass-filtered global SST data. Results, shown in Figs. 12a,c,e,g,i, indicate that the Atlantic–Pacific coupling is not stronger in the filtered data than it is in the unfiltered data. The same coupling is evident in patterns based on SST data in the Atlantic domain only, shown in Figs. 12b,d,f,h,j. Hence, the (albeit weak) Atlantic–Pacific coupling cannot be an artifact of mode mixing. The confinement of the PDO-like signature to the Pacific sector is likewise insensitive to low-pass filtering, as shown in Fig. 13.

It is evident from the lag correlation function between the AMO- and PDO-like modes, shown in Fig. 14, that the Atlantic–Pacific coupling is stronger if the latter is lagged relative to the former and that the strength of the lagged correlations increases markedly as the temporal

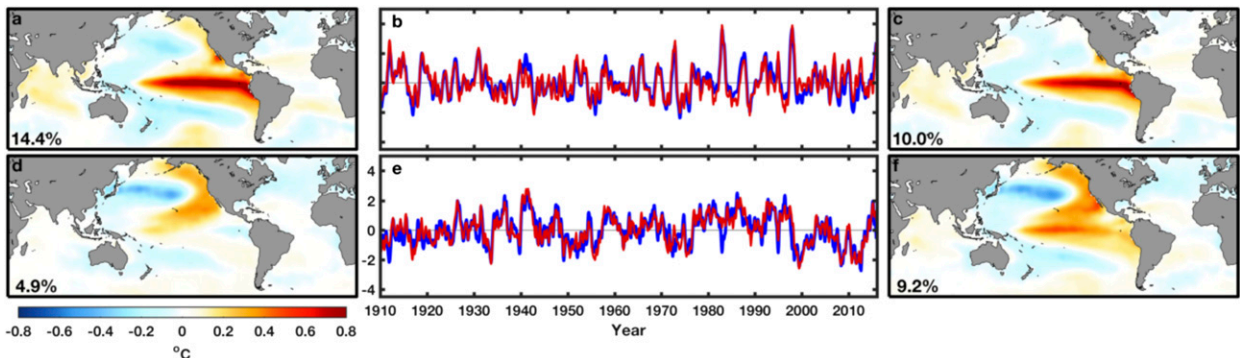


FIG. 9. Pairwise-rotated EOF2 and EOF4 of seasonal mean SST based on (a),(d) the SASC metric (18°) and (c),(f) the FASC metric (43°). (b),(e) The corresponding PCs are compared, with the blue line for the 18° rotation and the red line for the 43° rotation. Percentages of explained variance are printed at the bottom left on the EOF maps.

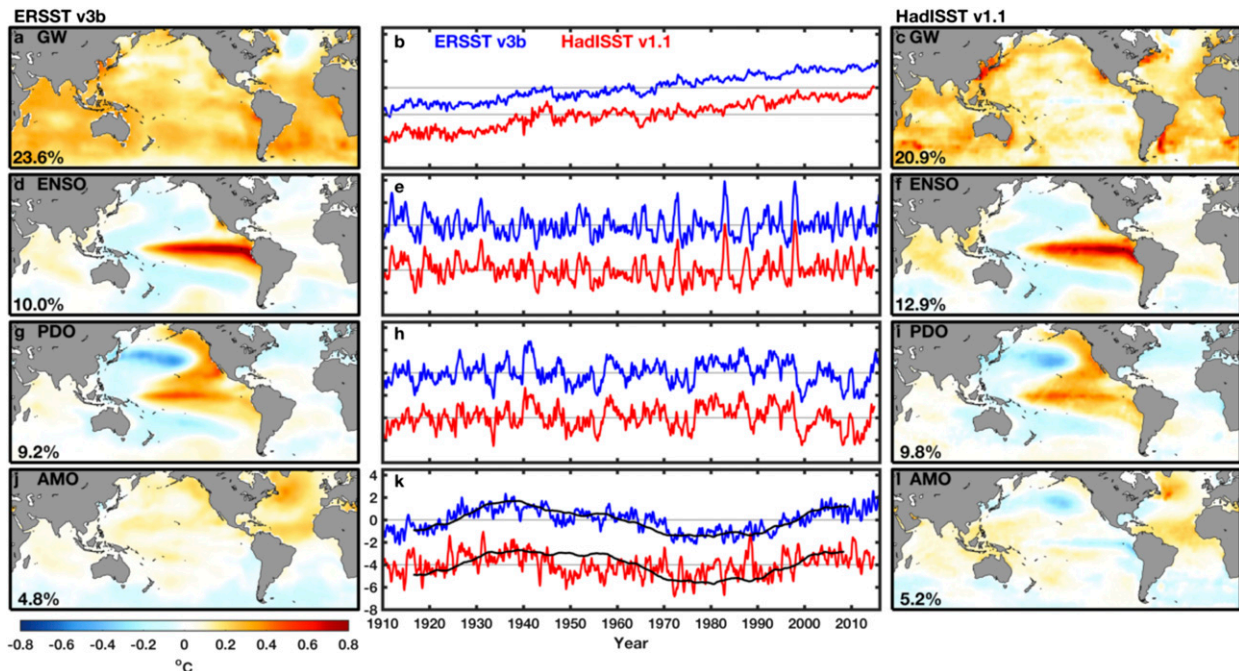


FIG. 10. The four leading rotated modes after performing all the rotations outlined in Fig. 2, based on (a),(d),(g),(j) ERSST.v3b and (c),(f),(i),(l) HadISST1.1, and (b),(e),(h),(k) the corresponding PCs. In (h), the index of our AMO-like mode is compared with the AMO index defined in Enfield et al. (2001), the detrended time series of SST averaged over the North Atlantic from the equator northward).

smoothing of the data is increased. In Fig. 14a, which is based on the pairwise-rotated PCs derived from the analysis of the global SST field, the simultaneous correlation is zero by construction, whereas in Fig. 14b, which is based on the PCs derived from the analyses in the separate oceans, the weak negative correlation at zero lag is consistent with the patterns in Figs. 12b,d,f,h,j. The recurrent SST pattern in Fig. 12 and the existence of pronounced peaks in both lag correlation functions at lags around ± 15 yr are consistent with prior results of Zhang and Delworth (2007), d'Orgeville and Peltier (2007), and Barcikowska et al. (2017). That the lag correlations are strongest in the 20-yr low-pass-filtered data at a lag of about 15 yr is consistent with the multi-decadal time scale (~ 60 -yr period) of the AMO. Owing to the limited length of the historical record, correlations relating to relationships on this time scale possess only a few statistical degrees of freedom and are hence not statistically significant. This does not preclude the possibility that they might nonetheless be indicative of true Atlantic–Pacific coupling as described in the references cited above.

e. The dynamical contribution to variations in detrended GSST

The dynamical contribution to variations in GSST of the ENSO-, PDO-, and AMO-like modes is shown in Fig. 15. These curves differ from those shown in Fig. 8

only in that PC2 and PC4 in Fig. 8 have been pairwise rotated. By virtue of its relatively large spatial mean and its long time scale, the AMO-like mode makes the largest contribution to the interdecadal variability of

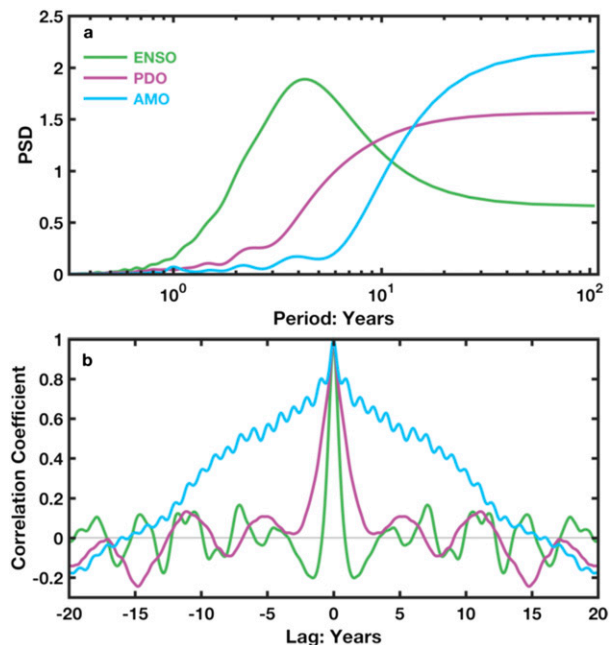


FIG. 11. (a) Power spectra and (b) autocorrelation functions for the ENSO-, PDO-, and AMO-like indices. The power spectra are normalized such that the area below each of them is the same.

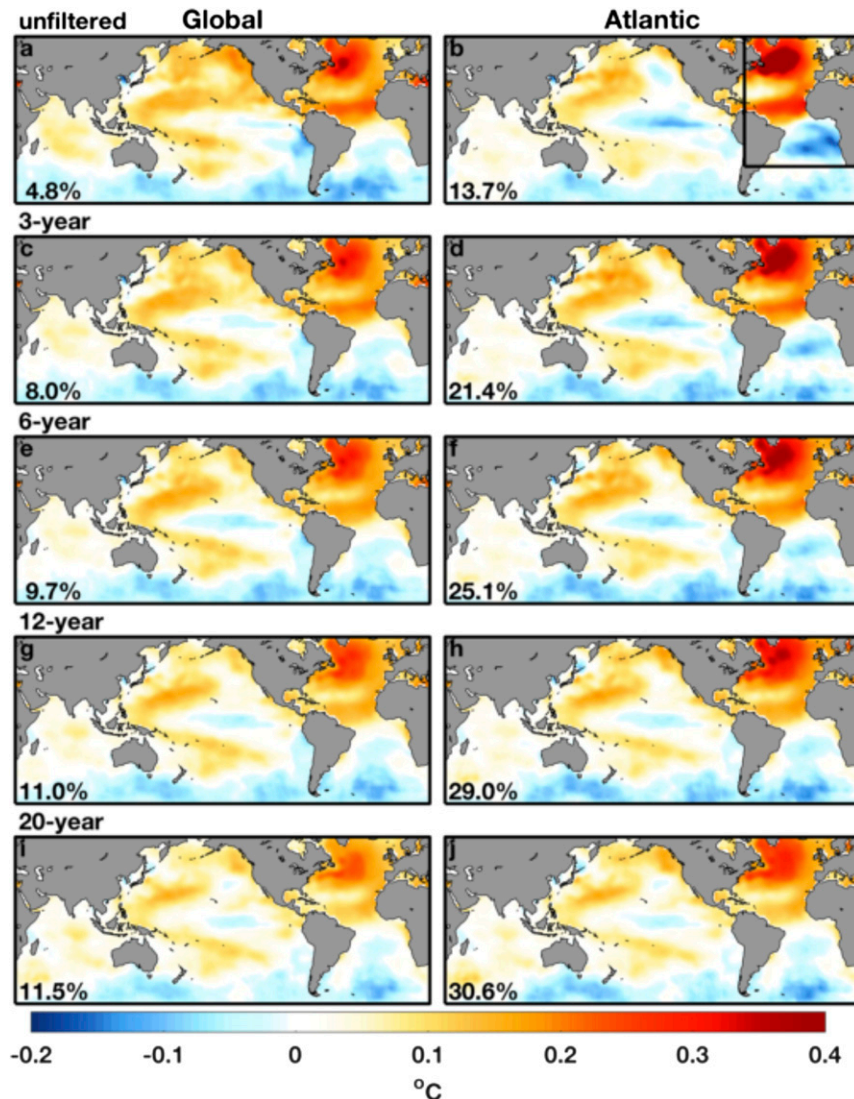


FIG. 12. (a) The AMO-like EOF4 of global SST after completing all the steps in the pairwise rotation protocol outlined in Fig. 2. (b) The AMO-like EOF2 of Atlantic (35°S – 65°N) SST after trend transfer with the global warming mode EOF1. Subsequent panels show the corresponding pairwise-rotated EOFs of low-pass-filtered SST fields, as indicated. Percentages of explained variance are printed at the bottom left on the EOF maps.

GSST, in agreement with results of Wu et al. (2011). However, in view of the limited number of temporal degrees of freedom inherent in the time-varying index of the AMO-like mode and our ad hoc assumption that it does not exhibit a linear trend, our statistical analysis cannot be regarded as providing definitive proof of the dominance of Atlantic multidecadal variability in modulating the rate of rise of GSST. Nor can we conclude, based on the very small SST global average of the PDO mode, that its contribution to the global mean land plus ocean surface temperature is small, being mindful of its close association with the atmospheric Pacific–North

American (PNA) pattern, which exerts a strong influence on the spatial mean surface air temperature over North America.

4. Summary and discussion

After pairwise rotations (i) between EOF3 and EOF4 to eliminate mixing between Atlantic and Pacific patterns (performed on the EOFs based on monthly mean data but not required for the EOFs based on seasonal mean data) and (ii) between the predominantly global warming mode EOF1 and the predominantly dynamical

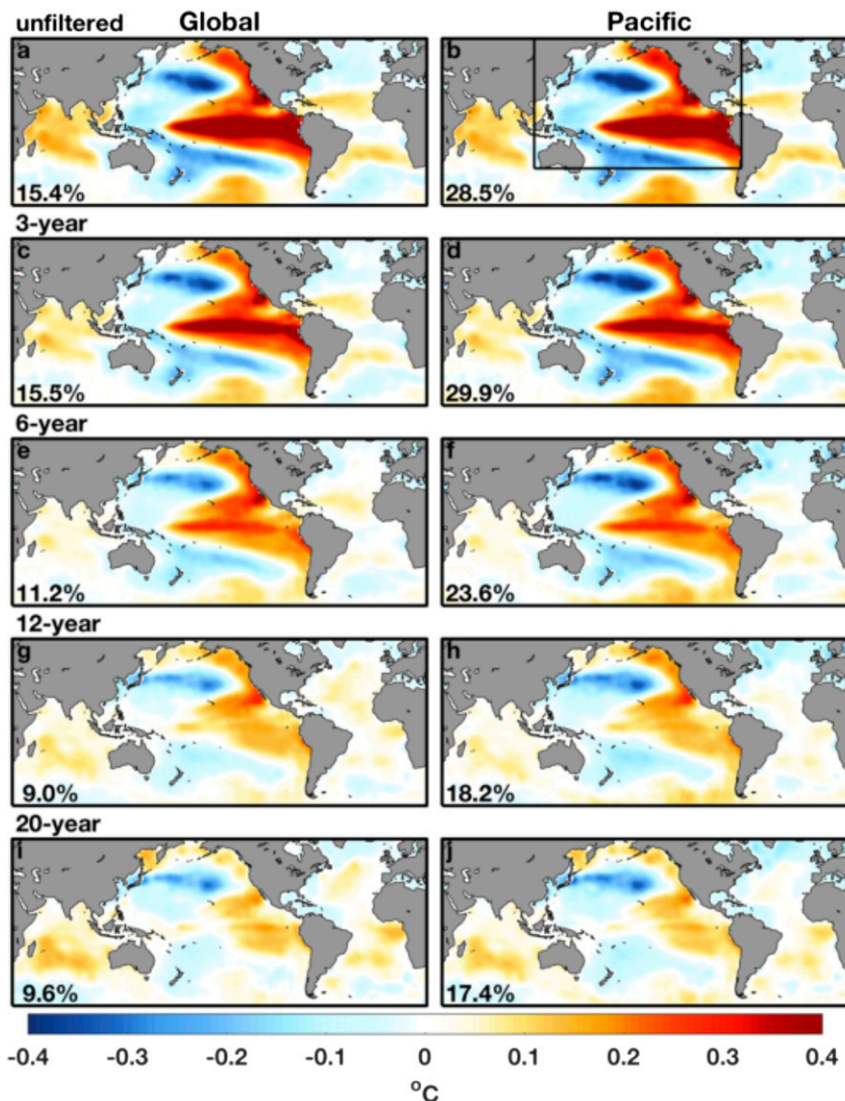


FIG. 13. As in Fig. 10, but for the (a),(c),(e),(g),(i) PDO-like EOF3 of global SST and (b),(d),(f),(h),(j) PC3 of Pacific (35°S–65°N) after trend transfer with the global warming EOF1 and a 45° rotation with EOF2 as in CW16.

modes 2–4 to transfer the trends in PC2–4 to PC1, and (iii) the rotation of the two Pacific modes based on the FASC criterion, we obtain the rotated modes shown in Figs. 10a,b,d,e,g,h,j,k. The PC of the leading mode resembles the GSST time series after the variability associated with PC2–4 has been regressed out. PC2 represents the ENSO-related variability in the equatorial belt. It is well correlated with conventional ENSO indices like Niño-3.4 and the equatorial Pacific cold tongue index (CTI) but it places greater emphasis on short-lived El Niño events and EOF2 is more equatorially focused than the regression pattern associated with conventional ENSO indices. The rotation tends to suppress the teleconnections between equatorial and

higher latitude SST in one-point correlation maps. As noted in the previous section, PC3 (based on FASC metric) is virtually identical to the PDO index and PC4 is virtually equivalent to the AMO index of Enfield et al. (2001; the detrended time series of 10-yr low-pass-filtered SST averaged over the North Atlantic from the equator northward).

Pairwise-rotated EOF2 and EOF3 are virtually identical to the modes obtained by CW16 by a 45° pairwise rotation of the two leading EOFs of SST* in the pan-Pacific domain. That their PCs exhibit such different frequency spectra—the more equatorially trapped mode with its variance concentrated on the interannual time scale and the PDO-like mode with its much redder

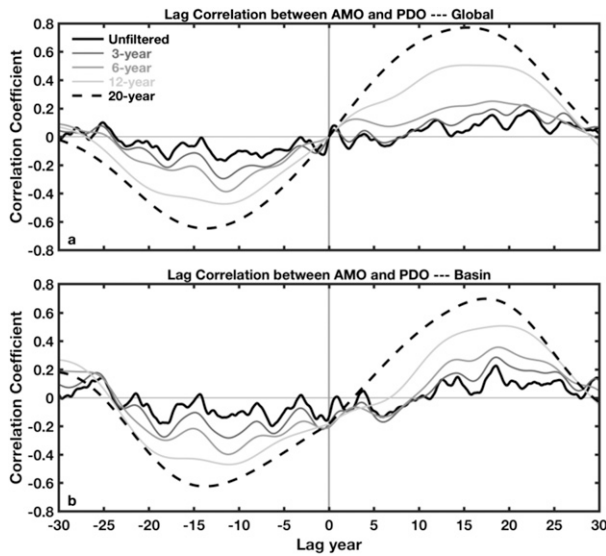


FIG. 14. The lag correlations (a) between AMO-like and PDO-like rotated EOFs of global low-pass-filtered SST and (b) between the PC2s of pan-Atlantic and pan-Pacific low-pass-filtered SST.

spectrum (Fig. 11a)—is further evidence that they correspond to physical processes whose temporal variability is linearly independent. The more equatorially trapped mode embodies the characteristics of the ENSO cycle as simulated in tropical models with active equatorial ocean dynamics, whereas the PDO-like mode, with its strong linkage with the atmospheric PNA pattern (CW16, their Fig. 4), resembles ENSO-like variability as simulated in global coupled models with slab oceans (Kitoh et al. 1999; Dommenges and Latif 2008; Clement et al. 2011).

It was shown in section 3a that whether the analysis is based on monthly or seasonal mean data affects the

analysis protocol, but not the final outcome of the analysis. Table 2 compares results obtained by applying a variety of analysis protocols to the same dataset. The analysis protocols differ from dataset to dataset but the final outcome is very similar. Comparison of the left and right panels of Fig. 12 (Fig. 13) shows that virtually identical AMO-like (PDO like) modes are obtained from an analysis of Atlantic (Pacific) SST. These same figures demonstrate the insensitivity of the analysis to low-pass filtering out to a 20-yr cutoff.

Performing the analysis on the HadISST dataset (Rayner et al. 2003) yields the pairwise-rotated EOFs shown in Figs. 10c,f,i,l. Compared to the ERSST results, the global warming signal in EOF1 is much more concentrated in the western boundary currents. The spatial inhomogeneity of the warming has been noted by Wu et al. (2012), who interpreted it as the signature of a strengthening and poleward migration of the currents in response to systematic changes in surface wind patterns in both Northern and Southern Hemispheres. The Pacific modes are very similar in the ERSST and HadISST datasets but the AMO-like mode is weaker in HadISST: its spatial pattern extends into all three oceans and it exhibits much more variability on time scales shorter than multidecadal.

Performing the analysis on the data from 1951 onward yields the results shown in Fig. 16. The only important difference between the patterns based on 1910–2015 versus 1951–2015 is that the AMO-like mode based on the shorter record is weaker.

We also performed an extensive series of comparisons of our results of pairwise rotation with those derived from varimax rotation. Figure 17 shows the modes obtained by rotating EOF1–20 and EOF2–20, which are typical of the varimax solutions when an appreciable

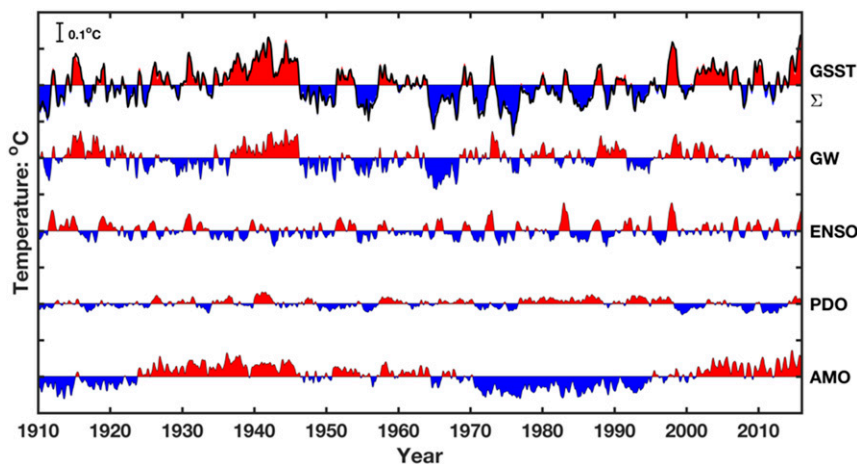


FIG. 15. As in Fig. 8, but after the application of step (iii) in the pairwise rotation protocol outlined in Fig. 2. The label Σ denotes the sum of the GW, ENSO, PDO, and AMO.

TABLE 2. Correlation matrix for rotated dynamical modes ENSO, PDO, and AMO during 1910–2015 and their associated spatial regression patterns. SST is global SST anomaly field; SST (1900–2015) means the analysis period is extended back to 1900 but the correlation coefficients are computed over 1910–2015. SST* is the global SST anomaly with the global mean SST removed from each grid point. SST# is the global SST anomaly with the linear trend of global mean SST removed from each grid point.

		SST (1910–2015)		SST (1900–2015)		SST* (1910–2015)		SST# (1910–2015)	
		Monthly	Seasonal	Monthly	Seasonal	Monthly	Seasonal	Monthly	Seasonal
Spatial	ENSO	1.00	0.99	0.99	0.96	0.94	0.97	0.98	0.99
	PDO	1.00	0.99	0.98	0.94	0.93	0.96	0.96	0.98
	AMO	1.00	0.99	0.95	0.89	0.74	0.82	0.85	0.83
Temporal	ENSO	1.00	0.97	0.98	0.93	0.88	0.93	0.97	0.98
	PDO	1.00	0.97	0.97	0.91	0.85	0.90	0.94	0.95
	AMO	1.00	0.97	0.97	0.86	0.74	0.81	0.86	0.84
Whether PC3 and PC4 are rotated		Yes	No	Yes	Yes	Yes	Yes	No	No

number of modes beyond the first four are included in the rotation. The results can be summarized as follows:

- When the global warming mode EOF1 is included in the analysis, it mixes with the ENSO-like EOF2.
- None of the varimax modes resembles our PDO-like pairwise-rotated mode based on the FASC criterion shown in Fig. 9f, but one of them closely resembles its counterpart based on the SASC criterion, shown in Fig. 9d.
- The varimax-rotated AMO-like mode is more concentrated near its primary center of action to the east of Newfoundland than in our AMO-like mode and its PC time series is not as dominated by multidecadal variability.

- Varimax rotation of modes 2–4 yields modes very similar to our pairwise-rotated modes based on the SASC criterion (not shown).
- Modes analogous to all three of our pairwise-rotated modes can be obtained by pairwise rotation of the varimax modes (not shown).

Subjective pattern recognition (i.e., identifying our pairwise-rotated modes with ENSO, the PDO, and the AMO) played a role in framing this paper (e.g., in labeling the modes) but the only way in which it guided the analysis was in justifying our conservative decision to retain the rotated Pacific modes based on both the SASC and FASC criteria. Had we not been aware of previous

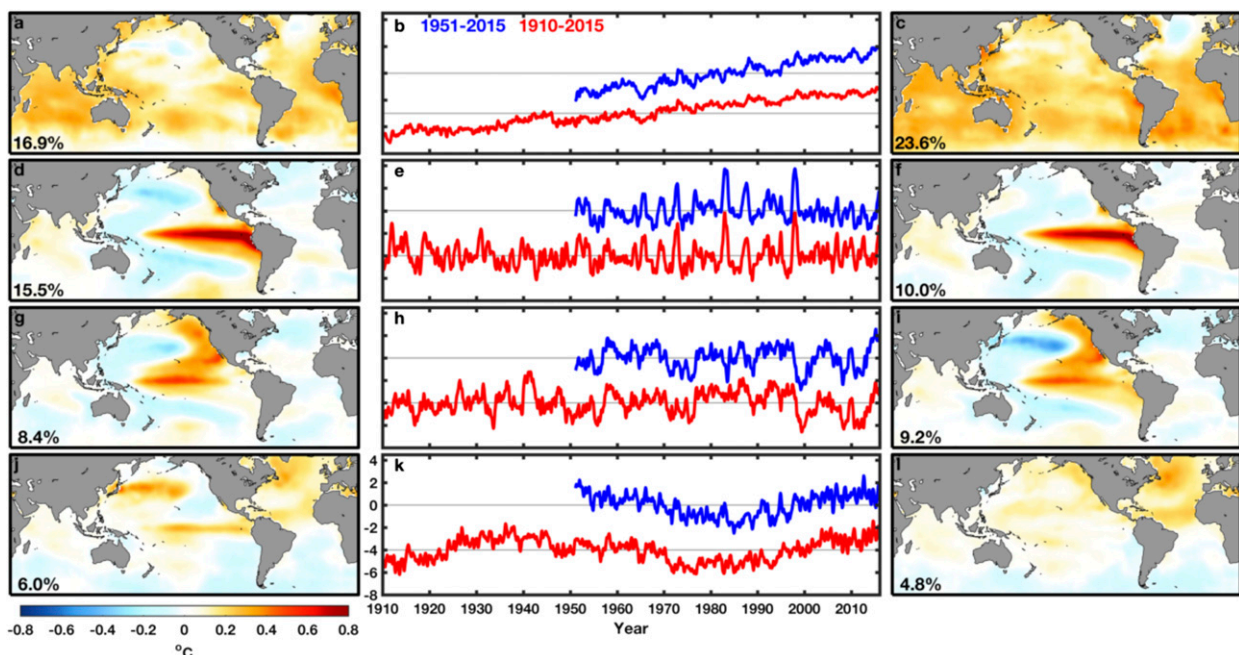


FIG. 16. (left) As in Fig. 10, but for ERSST.v3b from 1951 onward. (c),(f),(i),(l) As in Figs. 10a,d,g,j.

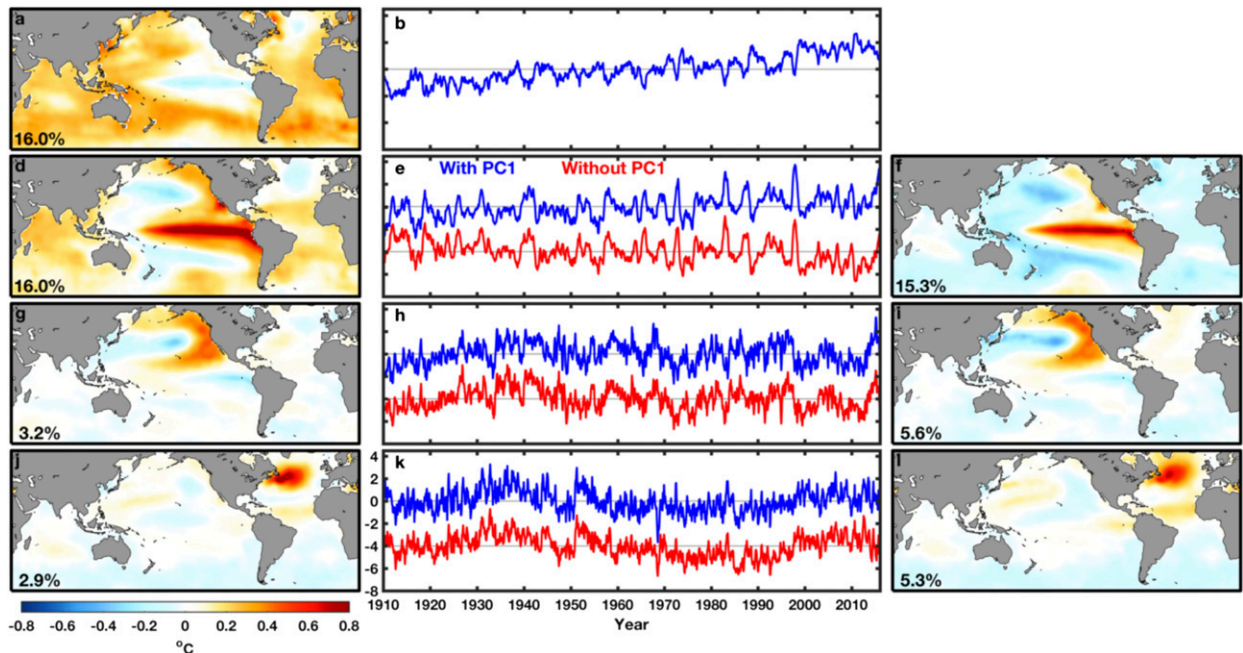


FIG. 17. First four modes obtained by varimax rotation of (a),(d),(g),(j) EOF1–20 and (f),(i),(l) EOF2–20 of monthly mean global SST, and (b),(e),(h),(k) their corresponding PC time series. There is no (c) because there is no corresponding case to (a).

studies of the PDO, we might very well have made the same decision, in which case we would have “discovered” the PDO, or two variants thereof. In favoring the FASC solution, we have given precedence to modes with minimal overlap in the frequency domain, as opposed to the space domain. As justification, we note that most analysts are more willing to sacrifice the spatial orthogonality of the EOFs than the temporal orthogonality of the PCs in choosing how to rotate EOFs.

Our FASC criterion is an extension of the notion of temporal orthogonality to the frequency domain. To apply it requires an a priori specification of the digital filters to be used in evaluating our temporal covariance metric FASC. It works well for separating ENSO and the PDO because the distinction between their characteristic time scales is well captured by the filters in Fig. 1. In general, the performance of pairwise rotations based on minimizing FASC is limited by the fact that most geophysical phenomena occupy broad and often overlapping ranges of the frequency spectrum and are therefore difficult to separate. Analysis techniques based on filtering in the frequency domain are subject to the same limitation.

Rotations based on the trend transfer algorithm can eliminate the mode mixing that occurs whenever secular trends and oscillatory modes of variability are superimposed. Mode mixing of this kind is evident not only in SST data but also in tropospheric temperature field derived from the microwave sounding unit (Santer et al.

2017) and in sea level data (Lombard et al. 2005). Rotations based on minimizing a FASC metric analogous to the one defined in this study may prove useful for extricating oscillatory phenomena in different frequency ranges without recourse to filtering in the frequency domain.

Acknowledgments. We wish to thank Shoshiro Minobe for his numerous helpful comments and suggestions for improving the clarity of the explanations of the methodology. Comments of an anonymous reviewer were also very helpful. JMW was supported by the U.S. National Science Foundation under Grant ATM 1122989. KKT was supported by the U.S. National Science Foundation under AGS-1262231 and DMS-940342. XC was supported by the Natural Science Foundation of China under Grants 41521091 and 41330960 and the Natural Science Foundation of China–Shandong Joint Fund for Marine Science Research Centers under Grant U1406401.

REFERENCES

- Barcikowska, M. J., T. R. Knutson, and R. Zhang, 2017: Observed and simulated fingerprints of multidecadal climate variability and their contributions to periods of global SST stagnation. *J. Climate*, **30**, 721–737, doi:10.1175/JCLI-D-16-0443.1.
- Barlow, M., S. Nigam, and E. H. Berbery, 2001: ENSO, Pacific decadal variability, and U.S. summertime precipitation, drought, and stream flow. *J. Climate*, **14**, 2105–2128, doi:10.1175/1520-0442(2001)014<2105:EPDVAU>2.0.CO;2.

- Bretherton, C. S., M. Widmann, V. P. Dymnikov, J. M. Wallace, and I. Bladé, 1999: The effective number of spatial degrees of freedom of a time-varying field. *J. Climate*, **12**, 1990–2009, doi:10.1175/1520-0442(1999)012<1990:TENOSD>2.0.CO;2.
- Chen, X., and J. M. Wallace, 2015: ENSO-like variability: 1900–2013. *J. Climate*, **28**, 9623–9641, doi:10.1175/JCLI-D-15-0322.1.
- , and —, 2016: Orthogonal PDO and ENSO indices. *J. Climate*, **29**, 3883–3892, doi:10.1175/JCLI-D-15-0684.1.
- Chiang, J. C. H., and D. J. Vimont, 2004: Analogous Pacific and Atlantic meridional modes of tropical atmosphere–ocean variability. *J. Climate*, **17**, 4143–4158, doi:10.1175/JCLI4953.1.
- Clement, A., P. Dinezio, and C. Deser, 2011: Rethinking the ocean’s role in the Southern Oscillation. *J. Climate*, **24**, 4056–4072, doi:10.1175/2011JCLI3973.1.
- Czaja, A., and C. Frankignoul, 2002: Observed impact of Atlantic SST anomalies on the North Atlantic Oscillation. *J. Climate*, **15**, 606–623, doi:10.1175/1520-0442(2002)015<0606:OIOASA>2.0.CO;2.
- Deser, C., and M. L. Blackmon, 1993: Surface climate variations over the North Atlantic Ocean during winter: 1900–1989. *J. Climate*, **6**, 1743–1753, doi:10.1175/1520-0442(1993)006<1743:SCVOTN>2.0.CO;2.
- , M. A. Alexander, S. P. Xie, and A. S. Phillips, 2010: Sea surface temperature variability: Patterns and mechanisms. *Annu. Rev. Mar. Sci.*, **2**, 115–143, doi:10.1146/annurev-marine-120408-151453.
- Dommenges, D., and M. Latif, 2008: Generation of hyper climate modes. *Geophys. Res. Lett.*, **35**, L02706, doi:10.1029/2007GL031087.
- , T. Bayr, and C. Frauen, 2013: Analysis of the non-linearity in the pattern and time evolution of El Niño southern oscillation. *Climate Dyn.*, **40**, 2825–2847, doi:10.1007/s00382-012-1475-0.
- d’Orgeville, and W. R. Peltier, 2007: On the Pacific decadal oscillation and the Atlantic multidecadal oscillation: Might they be related? *Geophys. Res. Lett.*, **34**, L23705, doi:10.1029/2007GL031584.
- Enfield, D. B., and A. M. Mestas-Núñez, 1999: Multiscale variabilities in global sea surface temperatures and their relationships with tropospheric climate patterns. *J. Climate*, **12**, 2719–2733, doi:10.1175/1520-0442(1999)012<2719:MVIGSS>2.0.CO;2.
- , —, and P. J. Trimble, 2001: The Atlantic Multidecadal Oscillation and its relation to rainfall and river flows in the continental U.S. *Geophys. Res. Lett.*, **28**, 2077–2080, doi:10.1029/2000GL012745.
- Folland, C. K., D. E. Parker, A. W. Colman, and R. Washington, 1999: Large scale modes of ocean surface temperature since the late nineteenth century. *Beyond El Niño: Decadal and Interdecadal Climate Variability*, A. Navarra, Ed., Springer, 73–102.
- Guan, B., and S. Nigam, 2008: Pacific sea surface temperatures in the twentieth century: An evolution-centric analysis of variability and trend. *J. Climate*, **21**, 2790–2809, doi:10.1175/2007JCLI2076.1.
- , and —, 2009: Analysis of Atlantic SST variability factoring interbasin links and the secular trend: Clarified structure of the Atlantic multidecadal oscillation. *J. Climate*, **22**, 4228–4240, doi:10.1175/2009JCLI2921.1.
- Jamison, N., and S. Kravtsov, 2010: Decadal variations of North Atlantic sea surface temperature in observations and CMIP3 simulations. *J. Climate*, **23**, 4619–4636, doi:10.1175/2010JCLI3598.1.
- Jolliffe, I. T., 1987: Rotation of principal components: Some comments. *J. Climatol.*, **7**, 507–510, doi:10.1002/joc.3370070506.
- Kaiser, H. F., 1958: The varimax criterion for analytic rotation in factor analysis. *Psychometrika*, **23**, 187–200, doi:10.1007/BF02289233.
- Kitoh, A., T. Motoi, and H. Koide, 1999: SST variability and its mechanism in a coupled atmosphere–mixed-layer ocean model. *J. Climate*, **12**, 1221–1239, doi:10.1175/1520-0442(1999)012<1221:SVAIMI>2.0.CO;2.
- Latif, M., R. Kleeman, and C. Eckert, 1997: Greenhouse warming, decadal variability, or El Niño? An attempt to understand the anomalous 1990s. *J. Climate*, **10**, 2221–2239, doi:10.1175/1520-0442(1997)010<2221:GWDVOE>2.0.CO;2.
- Lian, T., and D. Chen, 2012: An evaluation of rotated EOF analysis and its application to tropical Pacific SST variability. *J. Climate*, **25**, 5361–5373, doi:10.1175/JCLI-D-11-00663.1.
- Lombard, A., A. Cazenave, P.-Y. Le Traon, and M. Ishii, 2005: Contribution of thermal expansion to present-day sea-level change revisited. *Global Planet. Change*, **47**, 1–16, doi:10.1016/j.gloplacha.2004.11.016.
- Mantua, N. J., S. R. Hare, Y. Zhang, J. M. Wallace, and R. C. Francis, 1997: A Pacific interdecadal climate oscillation with impacts on salmon production. *Bull. Amer. Meteor. Soc.*, **78**, 1069–1079, doi:10.1175/1520-0477(1997)078<1069:APICOW>2.0.CO;2.
- McCabe, G. J., and M. A. Palecki, 2006: Multidecadal climate variability of global lands and oceans. *Int. J. Climatol.*, **26**, 849–865, doi:10.1002/joc.1289.
- Messié, M., and F. Chavez, 2011: Global modes of sea surface temperature variability in relation to regional climate indices. *J. Climate*, **24**, 4314–4331, doi:10.1175/2011JCLI3941.1.
- Mestas-Núñez, A. M., and D. B. Enfield, 1999: Rotated global modes of non-ENSO sea surface temperature variability. *J. Climate*, **12**, 2734–2746, doi:10.1175/1520-0442(1999)012<2734:RGMONE>2.0.CO;2.
- Minobe, S., 1999: Resonance in bidecadal and pentadecadal climate oscillations over the North Pacific: Role in climatic regime shifts. *Geophys. Res. Lett.*, **26**, 855–858, doi:10.1029/1999GL900119.
- Newman, M., G. P. Compo, and M. A. Alexander, 2003: ENSO-forced variability of the Pacific decadal oscillation. *J. Climate*, **16**, 3853–3857, doi:10.1175/1520-0442(2003)016<3853:EVOTPD>2.0.CO;2.
- , and Coauthors, 2016: The Pacific decadal oscillation, revisited. *J. Climate*, **29**, 4399–4427, doi:10.1175/JCLI-D-15-0508.1.
- Nigam, S., B. Guan, and A. Ruiz-Barradas, 2011: Key role of the Atlantic multidecadal oscillation in 20th century drought and wet periods over the Great Plains. *Geophys. Res. Lett.*, **38**, L16713, doi:10.1029/2011GL048650.
- North, G. R., T. L. Bell, R. F. Cahalan, and F. J. Moeng, 1982: Sampling errors in the estimation of empirical orthogonal functions. *Mon. Wea. Rev.*, **110**, 699–706, doi:10.1175/1520-0493(1982)110<0699:SEITEO>2.0.CO;2.
- Parker, D., C. Folland, A. Scaife, J. Knight, A. Colman, P. Baines, and B. Dong, 2007: Decadal to multidecadal variability and the climate change background. *J. Geophys. Res.*, **112**, D18115, doi:10.1029/2007JD008411.
- Quadrelli, R., C. S. Bretherton, and J. M. Wallace, 2005: On sampling errors in empirical orthogonal functions. *J. Climate*, **18**, 3704–3710, doi:10.1175/JCLI3500.1.
- Rayner, N. A., D. E. Parker, E. Horton, C. K. Folland, L. V. Alexander, D. P. Rowell, E. E. Kent, and A. Kaplan, 2003: Global analyses of sea surface temperature, sea ice, and night marine air temperature since the late nineteenth century. *J. Geophys. Res.*, **108**, 4407, doi:10.1029/2002JD002670.

- Richman, M. B., 1986: Rotation of principal components. *J. Climatol.*, **6**, 293–335, doi:10.1002/joc.3370060305.
- Santer, B. D., and Coauthors, 2017: Comparing tropospheric warming in climate models and satellite data. *J. Climate*, **30**, 373–392, doi:10.1175/JCLI-D-16-0333.1.
- Schlesinger, M. E., and N. Ramankutty, 1994: An oscillation in the global climate system of period 65–70 years. *Nature*, **367**, 723–726, doi:10.1038/367723a0.
- Shapiro, L. J., and S. B. Goldenberg, 1998: Atlantic sea surface temperatures and tropical cyclone formation. *J. Climate*, **11**, 578–590, doi:10.1175/1520-0442(1998)011<0578:ASSTAT>2.0.CO;2.
- Smith, T. M., R. W. Reynolds, T. C. Peterson, and J. Lawrimore, 2008: Improvements to NOAA's historical merged land-ocean temperature analysis (1880–2006). *J. Climate*, **21**, 2283–2296, doi:10.1175/2007JCLI2100.1.
- Takahashi, K., A. Montecinos, K. Goubanova, and B. Dewitte, 2011: ENSO regimes: Reinterpreting the canonical and Modoki El Niño. *Geophys. Res. Lett.*, **38**, L10704, doi:10.1029/2011GL047364.
- Thompson, D. W. J., J. J. Kennedy, J. M. Wallace, and P. D. Jones, 2008: A large discontinuity in the mid-twentieth century in observed global-mean surface temperature. *Nature*, **453**, 646–649, doi:10.1038/nature06982.
- Tourre, Y. M., S. Paz, Y. Kushnir, and W. B. White, 2010: Low-frequency climate variability in the Atlantic basin during the 20th century. *Atmos. Sci. Lett.*, **11**, 180–185, doi:10.1002/asl.265.
- Trenberth, K. E., and D. J. Shea, 2006: Atlantic hurricanes and natural variability in 2005. *Geophys. Res. Lett.*, **33**, L12704, doi:10.1029/2006GL026894.
- Wallace, J. M., C. Smith, and Q. Jiang, 1990: Spatial patterns of atmosphere–ocean interaction in the northern winter. *J. Climate*, **3**, 990–998, doi:10.1175/1520-0442(1990)003<0990:SPOAOI>2.0.CO;2.
- Weare, B. C., A. R. Navato, and R. E. Newell, 1976: Empirical orthogonal analysis of Pacific sea surface temperatures. *J. Phys. Oceanogr.*, **6**, 671–678, doi:10.1175/1520-0485(1976)006<0671:EOAOPS>2.0.CO;2.
- Wheeler, M. C., and H. H. Hendon, 2004: An all-season real-time multivariate MJO index: Development of an index for monitoring and prediction. *Mon. Wea. Rev.*, **132**, 1917–1932, doi:10.1175/1520-0493(2004)132<1917:AARMMI>2.0.CO;2.
- Wilks, D., 2011: *Statistical Methods in the Atmospheric Sciences*. Academic Press, 704 pp.
- Wu, L., and Coauthors, 2012: Enhanced warming over the global subtropical western boundary currents. *Nat. Climate Change*, **2**, 161–166, doi:10.1038/nclimate1353.
- Wu, Z., N. E. Huang, J. M. Wallace, B. V. Smoliak, and X. Chen, 2011: On the time-varying trend in global-mean surface temperature. *Climate Dyn.*, **37**, 759–773, doi:10.1007/s00382-011-1128-8.
- Yeo, S.-R., S.-W. Yeh, K.-Y. Kim, and W. Kim, 2017: The role of low-frequency variation in the manifestation of warming trend and ENSO amplitude. *Climate Dyn.*, doi:10.1007/s00382-016-3376-0, in press.
- Zhang, R., and T. L. Delworth, 2007: Impact of the Atlantic multidecadal oscillation on North Pacific climate variability. *Geophys. Res. Lett.*, **34**, L23708, doi:10.1029/2007GL031601.
- Zhang, W., J. Li, and X. Zhao, 2010: Sea surface temperature cooling mode in the Pacific cold tongue. *J. Geophys. Res.*, **115**, C12042, doi:10.1029/2010JC006501.
- Zhang, Y., J. M. Wallace, and D. S. Battisti, 1997: ENSO-like interdecadal variability: 1900–93. *J. Climate*, **10**, 1004–1020, doi:10.1175/1520-0442(1997)010<1004:ELIV>2.0.CO;2.